Injury, Int. J. Care Injured 50 (2019) 639–647

Contents lists available at ScienceDirect

Injury

journal homepage: www.elsevier.com/locate/injury

Genetic variation in mice affects closed femoral fracture pattern outcomes

Michal Bartnikowski[a], Nicole Bartnikowski[a], Anna Woloszyk[b], Romano Matthys[c], Vaida Glatt[a,b,*]

[a] Institute of Health and Biomedical Innovation, Queensland University of Technology, Brisbane, Queensland, Australia
[b] Department of Orthopaedics, University of Texas Health Science Center, San Antonio, TX, USA
[c] RISystem AG, Davos Platz, Switzerland

ARTICLE INFO

Keywords:
Closed transverse fracture
Bone morphology
Mouse strains
Fracture device
Murine model
Fracture
Mouse

ABSTRACT

The purpose of this study was to determine whether differences in structural and material properties of bone between different mouse strains influence the fracture patterns produced under experimental fracture conditions.

Femurs of C57BL/6 (B6), C3H/HeJ (C3H), and DBA/2 (DBA) strains were evaluated using micro-computed tomography (μCT), measurements derived from radiographic images and mechanical testing to determine differences in the geometry and mechanical properties. A fracture device was used to create femoral fractures on freshly sacrificed animals using a range of kinetic energies (~20–80 *mJ*) which were classified as transverse, oblique, or comminuted.

B6 femurs had the lowest bone volume/total volume (BV/TV) and bone mineral density (BMD), thinnest cortex, and had the most variable fracture patterns, with 77.5% transverse, 15% oblique, and 7.5% comminuted fractures. In contrast, C3H had the highest BV/TV, BMD, and thickest cortices, resulting in 97.5% transverse, 2.5% oblique, and 0% comminuted fractures. DBA had an intermediate BV/TV and thickness of cortices, with BMD similar to C3H, resulting in 92.9% transverse, 7.1% oblique, and 0% comminuted fractures. A binomial logistic regression confirmed that bone morphometry was the single strongest predictor of the resulting fracture pattern.

This study demonstrated that the reproducibility of closed transverse femoral fractures was most influenced by the structural and material properties of the bone characteristics in each strain, rather than the kinetic energy or body weight of the mice. This was evidenced through geometric analysis of X-ray and μCT data, and further supported by the bone mineral density measurements from each strain, derived from μCT. Furthermore, this study also demonstrated that the use of lower kinetic energies was more than sufficient to reproducibly create transverse fractures, and to avoid severe tissue trauma. The creation of reproducible fracture patterns is important as this often dictates the outcomes of fracture healing, and those studies that do not control this potential variability could lead to a false interpretation of the results.

Introduction

The majority of bone fractures heal spontaneously, but approximately 5–10% result in delayed unions, non-unions, or large bone defects, creating significant therapeutic challenges for surgeons. Numerous factors may lead to complications in fracture healing, including congenital disorders such as neurofibromatosis [1], poor mechanical stability [2], poor blood supply due to local soft tissue trauma [3,4], infection [5], smoking [6], osteoporosis [7,8], anemia [9], diabetes [10,11], and poor nutrition [12,13]. Over the past several decades, researchers have attempted to address these complications by characterizing the factors that most influence normal fracture healing.

Animal models have been used to assess various pathologies and to better understand the underlying mechanisms in order to develop more effective clinical treatments for diseases in humans and animals [14]. Both large animal models (*e.g.* primate [15,16], equine [17,18], ovine [19–21], and canine [22]), and small animal

* Corresponding author at: Department of Orthopedics, University of Texas Health Science Center San Antonio, 7703 Floyd Curl Drive – MC 7774, San Antonio, TX 78229-3900, USA.
E-mail address: glatt@uthscsa.edu (V. Glatt).

https://doi.org/10.1016/j.injury.2019.02.012
0020-1383/

models (*e.g.* rabbit [23,24], rat [25,26] and mouse [27–30]) have been employed for this purpose. Large animals remain the models of choice due to their similarities in bone healing mechanisms and physiological scale to humans. However, handling difficulties and the high costs associated with using large animal models have made them less attractive compared to small animal models.

Small animal models, particularly mice, have gained prominence in the study of fracture healing due to the availability of broad-spectrum molecular assays and the ability to generate transgenic animals, allowing for the study of genetic and molecular mechanisms in bone repair. Studies of fracture healing most commonly use the tibia and femur, with both having their respective advantages. Although the tibia provides the easiest access to bone, it lacks the level of soft tissue coverage present on the femur. Furthermore, the tibia also has a curved major axis that requires more complex mechanical testing regimens and subsequent analyses [31], and if the fibula becomes compromised during the surgical procedure, the healing outcome might be adversely affected. The femur thus provides the preferred framework for a closed transverse murine fracture model, which is the most common model of bone repair, and is produced by externally applied blunt trauma. This model is very similar to a common long bone fracture seen in the clinical setting in terms of etiology, anatomical site, and fixation method, and was therefore selected for this study [32,33].

Several efforts have been made to characterize the patterns of experimentally produced closed fractures in rodents [25,29,34–36]. These studies have demonstrated the reproducibility of transverse fracture rates of approximately 86%, with the main determining factor for variability not reported [29] or attributed to kinetic energy levels [34]. Notably, Manigrasso et al. [37] used a closed fracture model to determine the pattern of fracture healing in three strains of mice, however, the reproducibility and types of fracture produced by their device, and whether the fracture outcome was influenced by the strain of mouse investigated, was not reported. In contrast, the goal of the Marturano et al. [34] study was to present a murine femur fracture device that improves the quality and reproducibility of experimental closed fractures. This study found that it was possible to create reproducible closed transverse fractures in mouse femurs if both the mass and velocity (kinetic energy) were selected appropriately. These studies demonstrated that the creation of reasonably reproducible closed transverse fractures is possible, although difficulties included the positioning of the animal to attain a consistent fracture pattern, determining the amount of impact kinetic energy required, and understanding whether the same fracture conditions could be applied to different strains and sizes of mice.

Therefore, the main goal of this study was to determine whether the structural and material properties of bone resulting from genetic variations within specific mouse strains would influence the pattern of fracture outcomes. To this end, controlled experiments were performed to characterize the pattern of fractures created using three inbred strains of mice, C57BL/6 (B6), C3H/HeJ (C3H), and DBA/2 (DBA), all of which havewell-defined genetic backgrounds with a characteristic bone morphology. Those specific strains were selected due to their distinct differences in structural and material properties of bone, and furthermore, because they are the most commonly investigated strains to study the influence of genetic variation on fracture healing [37,38]. To create reproducible closed transverse fractures in mouse femurs, a novel fracture device designed specifically for this purpose was used. We hypothesized that the differences in structural and material properties would influence the fracture outcomes observed, and the reproducibility of closed transverse fractures would depend on both the impact kinetic energy and the body weight of mice.

Methods

Experimental study design

A pilot study was conducted using μCT scans of C57BL/6 (B6; $n = 11$), C3H/HeJ (C3H; $n = 12$), and DBA/2 (DBA; $n = 10$) mouse femurs of male mice aged between 10 to 12 weeks, to assess geometry and bone mineral density prior to X-ray imaging and fracture creation. This was performed to determine if the values of bone geometrical properties derived from 2D X-ray images would correspond to those obtained from μCT. This correlation was critical to ensure that X-ray data could be used for an accurate evaluation of geometric values of bone. The use of μCT for post-fracture assessment was not feasible as femurs would have been required to be explanted from the body prior to scanning, and this would have disturbed the fracture alignment. Furthermore, the use of μCT to scan and analyze the large number of femurs that were required for this study would have been costly and time consuming compared to that of X-ray imaging.

For closed fracture experiments, 40 males each from B6 and C3H, and 42 males from DBA strains, aged between 10 to 12 weeks were used. Fractures were created immediately after euthanasia to minimize the effects of *rigor mortis*. All animal procedures were followed in accordance of IACUC protocols, despite being performed *post mortem*.

The Rodent Fracture Device (RFD; RISystem AG, Davos Platz, Switzerland) was used to create closed transverse fractures in mice femurs (Fig. 1). To do this, a small longitudinal incision was made on the right hind limb over the surface of the patella, extending towards the medial quadriceps muscle and through the fascia. Care was taken to ensure minimal soft tissue damage. The patella was dislocated laterally to expose the distal end of the femur and proximal end of the tibia. A 27 G hypodermic needle was used to create a small hole at the end of the femur, concentric with the

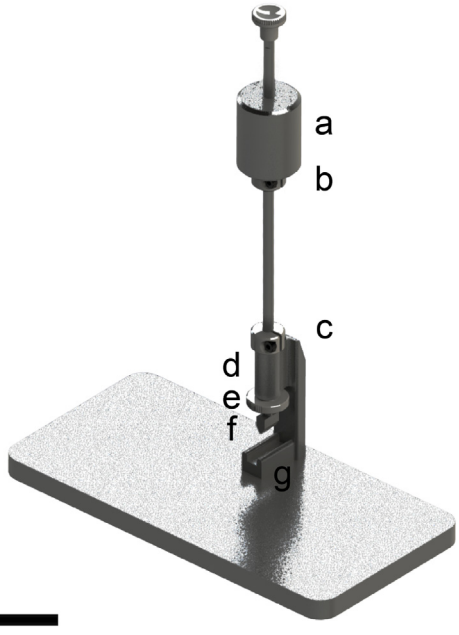

Fig. 1. Schematic illustration of the Rodent Fracture Device. The Rodent Fracture Device is made of stainless steel (grade 304/1.4301). The system consists of a low-friction bearing within a metallic sleeve (d) which guides the shaft along a vertical path. The top screw adjustment (b) allows the control of the drop-height for the weight (a). The bottom screw adjustment (c) controls the penetration depth of the striker (f) between the anvils (g), while the knurled disc (e) allows for pre-loading of the specimen prior to fracture. Scale bar = 5 *cm*.

medullary canal, to penetrate through the marrow canal. A 30 G tungsten alloy wire was then inserted into the medullary canal of the femur through the distal hole, and extended about 20 *mm* outside through the proximal and distal ends, to keep the alignment of the femur during and after the fracture [29,30,34]. It is important to note that this wire did not serve as the fixation device to stabilize the fracture. The mouse was placed in the supine position, with the tail and target limb on one side of the main column of the device. The distal end of the tibia was aligned with the base of the tail, with the femur centered on the anvil supports. The striker was lowered down onto the target site and aligned parallel on the anvil supports, then the knurled nut was adjusted to provide a secure contact to the femur and to hold the alignment in place. The weight was then carefully raised to the predetermined height and allowed to drop freely onto the femur to create a fracture. To create transverse fractures, various drop-heights were used, the details of which are provided in Table 1. A penetration depth of 1 *mm* was used for all groups, as recommended by the manufacturer. Immediately post-fracture, all femurs were imaged in the posterior-anterior plane using radiography. Fracture types were classified as either transverse, oblique, or comminuted by an independent blinded evaluation conducted by three individuals. Mouse weight, drop-height, and fracture pattern outcomes were recorded for each femur.

Micro-computed tomography (μCT)

A desktop μCT imaging system (μCT40, Scanco Medical AG, Bassersdorf, Switzerland) equipped with a 10 *mm* focal spot microfocus X-ray tube, at a 12 μm isotropic voxel size, 75 *keV* energy and 200 *ms* integration time were used to scan mouse femurs (50 μCT slices per specimen). Evaluation was performed using all of the slices scanned in the midshaft femur. The following variables were assessed: total volume (TV, mm^3), bone volume (BV, mm^3), bone volume/total volume (BV/TV, %), cortical thickness (CtTh, *mm*), bone mineral density (BMD, $mgHA{\cdot}cm^{-3}$), and polar moment of inertia (pMOI, mm^4). Images were thresholded using an algorithm and morphometric variables computed from the binarized images using direct 3D techniques that do not rely on any prior assumptions about the underlying structure.

X-ray imaging

The same femurs used for μCT and for the closed transverse fracture experiments were imaged in the posterior-anterior plane using a Faxitron MX-20 cabinet X-ray system (Faxitron X-ray LLC; Wheeling, IL, USA), and prior to dissection for μCT scanning. The outer (OD) and inner diameters (ID) were measured on the X-ray images using ImageJ software (National Institutes of Health, Bethesda, MD, USA). Measurements were taken at the middle of the femur, approximately 1 *mm* from the end of the greater trochanter. Dimensional measurements were performed three times, and an average value for each sample was used. Cortical thickness (CtTh, *mm*), bone area (BA, mm^2), total area (TA, mm^2), and bone area/total area ratio (BA/TA, %) were calculated from the X-ray measurements assuming a circular cross-section.

Table 1
Experimental study conditions.

Drop-height, h (*mm*)	Impact velocity, $v(m.s^{-9})$	Impact kinetic energy, E_k (*mJ*)
10	0.443	19.6 (~20)
15	0.542	29.4 (~30)
20	0.620	39.2 (~40)
25	0.700	49.1 (~50)
30	0.767	58.9 (~60)
35	0.829	68.7 (~70)
40	0.886	78.5 (~80)

Ex vivo torsional testing

Five femurs from each mouse strain were used for mechanical testing. The end of each femur was embedded in poly(methyl methacrylate) (PMMA) bone cement (Parapress® vario, Kulzer, USA) and tested to failure using a torsional testing device in conjunction with an Instron MicroTester 5848 material testing system (Instron, MA, USA), at a $1^{\circ}{\cdot}s^{-1}$ strain rate using a 100 *N* load cell. Angular deformation and applied load data were acquired at 10 *Hz* and used to calculate maximum torque (T_{max}, $N \cdot mm$), torsional rigidity (w_T, $N \cdot mm^2$) and shear modulus (G, *MPa*) of the femurs. Torsional testing was chosen to determine mechanical properties of bone, because it is the most common loading condition under which fractures occur in humans. This outcome measure was not used to simulate transverse fracture creation, but rather to evaluate bone strength, rigidity and shear modulus of each strain.

Rodent fracture device

The RFD is a gravity-driven three-point bending system, comprising a mass with an adjustable drop-height delivering a consequent kinetic energy, as well as an adjustable striker penetration depth and drop-weight mass, along with set anvil spacing (Fig. 1). The RFD was designed to minimize user-controlled variables. To achieve this, fracture conditions were purely reliant on the manipulation of the drop-height and penetration depth. While both of these are adjustable, the penetration depth of the striker was shown to be of critical importance in creating reproducible fractures, and insufficient penetration could lead to variable fracture outcomes [39]. Hence, it was maintained at a fixed depth of 1 *mm* interference.

To create a facture, the striker is held in the vertical plane by a low-friction sleeve with two adjustable screw sleeves along the length of the shaft. The top adjustment regulates the drop-height of the weight, whereas the bottom adjustment regulates the penetration depth of the striker between the two anvils. The knurled nut directly above the striker is used for securing the target limb for stabilization prior to fracture.

The magnitude and distribution of fracture energy delivered to a target site is a major factor in determining the type of fracture that will be created. The main variables of the RFD are: weight (w) 200 *g*, drop-height (h) penetration depth, a range of 0-105 *mm* (d) striker and anvil edge rounding, a range of +2/-5 *mm*, and the (r) anvil spacing, 2 *mm*, with (s) set at 9 *mm* center to center. Striker velocity is calculated assuming free-fall conditions as shown in Eq. 1, where v is velocity ($m{\cdot}s^{-1}$), g is the gravity constant, and h is the release height [4].

$$v = \sqrt{2gh} \tag{1}$$

The magnitude of kinetic energy delivered by the fracture device to a femur is exclusively dependent upon the drop-height and velocity, as shown in Eq. 2, where E_k is kinetic energy, m is the mass of the weight, and v is the velocity of the weight upon impact.

$$E_k = \frac{1}{2}mv^2 \tag{2}$$

The limits of the device were calculated at a velocity range of 0-1.435 $m{\cdot}s^{-1}$, and a kinetic energy range of 0–206 *mJ*. The use of an appropriate level of kinetic energy is critical in achieving reproducible closed transverse fractures.

Data analysis

Data was analyzed using SPSS 23.0 (IBM SPSS Statistics, IBM Corporation; Endicott, NY, USA). A binomial logistic regression model was used to test the potential predictive capacity of the data set. Analysis was performed on the outcomes, with oblique and comminuted fractures considered as failures. The analysis was conducted using kinetic energy, body weight, and BA/TA measured from X-rays (40–42 samples per variable).

Prior to analysis, data was first processed to ensure that logistic regression assumptions were met. A Box-Tidwell test was used to determine the presence of a linear relationship between the dependent variable and any continuous predictors. A Bonferroni correction was applied using all 7 terms of the model, with significance being accepted when $p < 0.007$. Analysis of variance (ANOVA) or t-tests were used to assess intergroup comparisons, $p < 0.05$ was considered significantly different for all analyses.

Results

The μCT data showed that C3H had a significantly higher (~160%) BV than the other strains ($p < 0.0001$; Fig. 2A), but it was not different between B6 and DBA. TV was the highest in B6, intermediate in C3H, and the lowest in DBA, and was significantly different between all of the groups ($p < 0.0001$; Fig. 2B). B6 had the lowest BV/TV, followed by DBA, with C3H having the highest, and was significantly different between all groups ($p < 0.0001$; Fig. 2C). B6 had the lowest BMD compared to DBA and C3H ($p < 0.0001$ *vs.* both), while C3H and DBA were not different from each other (Fig. 2D).

Mechanical testing showed significant difference in maximum torque between DBA and the other strains (B6 *vs.* DBA, $p = 0.04$; C3H *vs.* DBA, $p = 0.0005$), and while C3H was greater than B6, a significant difference was not reached ($p = 0.09$; Fig. 3A). Torsional rigidity demonstrated very similar results between B6 and C3H, where DBA was significantly lower than both strains ($p = 0.046$, $p = 0.028$, respectively; Fig. 3B). The lower polar moment of inertia in DBA femurs ($p < 0.0001$ *vs.* both B6 and C3H; Fig. 3C) also resulted in a significantly higher shear modulus ($p = 0.05$ *vs.* B6, $p = 0.03$ *vs.* C3H; Fig. 3D).

The same femurs were imaged using X-rays prior to dissection in order to compare the measurements derived from the X-ray images to those of μCT. Cortical thickness (CtTh) was the thinnest in B6, intermediate in DBA, and the thickest in C3H, and was significantly different between all groups ($p < 0.0001$; Fig. 4A). A comparison between X-ray and μCT measurements of the CtTh and BA/TA *vs.* BV/TV was performed to assess the accuracy of the X-ray measurements to the true dimensions of the femurs. The measurements from both imaging modalities had the same trends and were not significantly different (Fig. 4A, B), resulting in very strong correlations (Fig. 4C, D; $R^2 > 0.9$). This supported the use of X-ray measurements in the further analysis, reinforcing the reliability of the model.

In closed transverse fracture experiments, a significant difference was found in body weight between all three strains, as shown in Fig. 5A ($p < 0.0001$, weight range 21.8 33.8 *g*). Femur OD, CtTh, and BA/TA were also significantly different between all groups ($p < 0.0001$; Fig. 5B, C), while femur ID was only significantly different between B6 and C3H ($p < 0.0001$), and B6 and DBA ($p < 0.0001$) strains (Fig. 5B).

Interestingly, the reproducibility of transverse fractures did not depend upon the impact kinetic energy, and since there was no significant difference between the various conditions within each strain (Fig. 6A–C), the data was pooled for further analysis (Fig. 6D). Transverse fracture patterns were the most reproducible in C3H, followed by DBA, and B6. Fracture outcomes as a percentage of transverse, oblique, and comminuted fractures across the tested range of kinetic energies is shown in Fig. 6D and Table 2 (B6 *vs.* C3H, $p = 0.0064$; B6 *vs.* DBA, $p = 0.05$; C3H *vs.* DBA, $p = 0.34$), along with representative radiographs of the characteristic fracture patterns for each strain (Fig. 7).

A binomial logistic regression model was used to test the potential predictive capacity of the fracture pattern outcomes. The analysis was conducted using kinetic energy (E_k), body weight (w), and BA/TA measured from X-rays. This model accurately predicted 88.5% of all fractures, demonstrating a sensitivity of 46.2% and

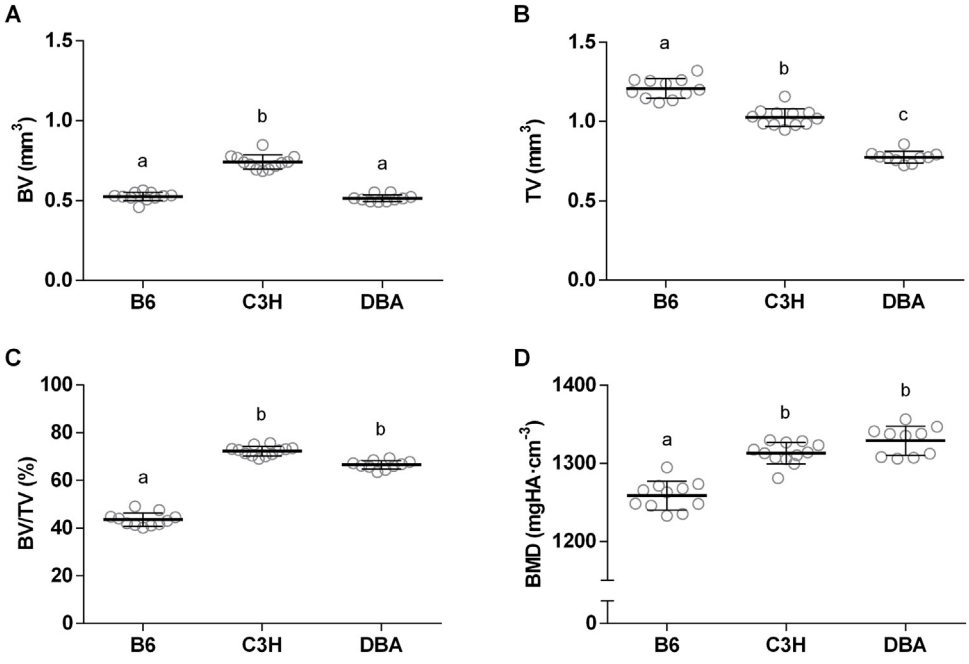

Fig. 2. Bone morphometric parameters from μCT analysis. A) Bone Volume (BV); B) Total Volume (TV); C) Bone Volume/Total Volume (BV/TV); D) Bone Mineral Density (BMD). Statistical significance is indicated for each panel. In each case, statistically similar groups share symbols, $n = 10$.

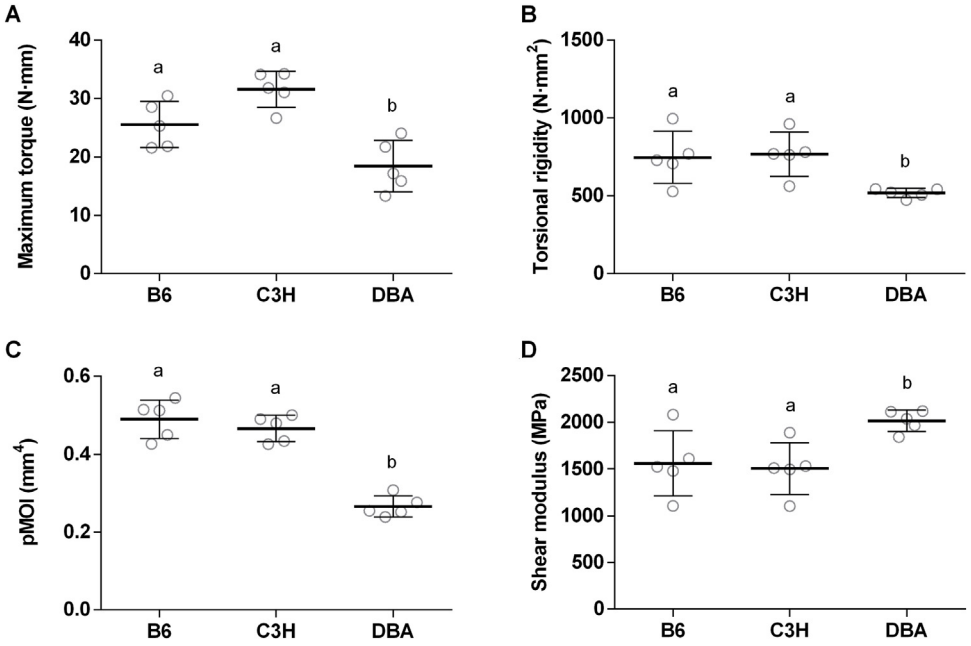

Fig. 3. Comparison of torsional mechanical properties of mouse femurs in B6, C3H, and DBA strains. A) Maximum torque, $\boldsymbol{T_{max}}$; B) Torsional Rigidity, $\boldsymbol{w_T}$; C) Polar moment of inertia, (pMOI); and D) Shear modulus, $\boldsymbol{G}$, evaluated by μCT. Statistical significance is indicated for each panel. In each case, statistically similar groups share symbols, $n = 5$.

specificity of 93.6%. Of the three predictor variables, the model only identified significant contribution from BA/TA ($p = 0.004$), indicating that the greater the value of this variable, the greater likelihood of transverse fracture outcomes. This data illustrated that the creation of reproducible closed transverse fractures is possible in the presented mouse strains at various body weights, over a wide range of kinetic energies (~20 to ~80 *mJ*).

Discussion

The aim of this study was to investigate the reproducibility of closed transverse fractures across three genetic strains of mice (B6, C3H and DBA) using the RFD under various conditions. The resulting fracture patterns (transverse, oblique, or comminuted) were evaluated with respect to the influence of the impact kinetic

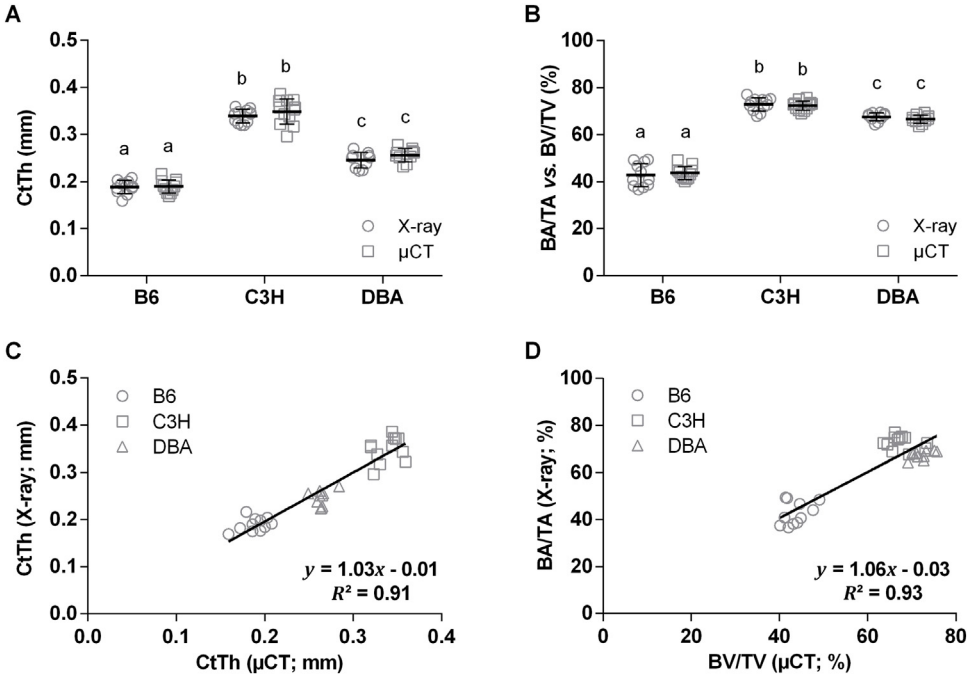

Fig. 4. Comparison and correlation of geometric parameters obtained from X-ray and μCT images in B6, C3H, and DBA strains. A) Cortical Thickness (CtTh); B) Bone Area/Total Area (BA/TA) *vs.* Bone Volume/Total Volume (BV/TV); C) Linear regression of CtTh comparing X-ray to μCT data; D) Linear regression of BA/TA *vs.* BV/TV comparing X-ray to μCT data. Statistically similar groups share symbols, $n = 10$.

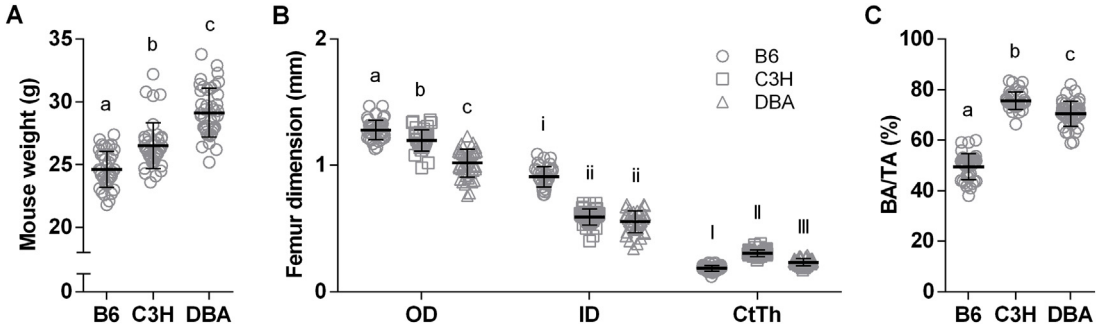

Fig. 5. Body weight and bone morphometric parameters in B6, C3H, and DBA strains. A) Mouse body weight; B) Femur dimensions of outer diameter (OD), inner diameter (ID), and cortical thickness (CtTh) as measured from X-ray images; and C) Bone area/Total area (BA/TA) calculated assuming a circular cross-section. Statistically similar groups share symbols, $n = 40–42$.

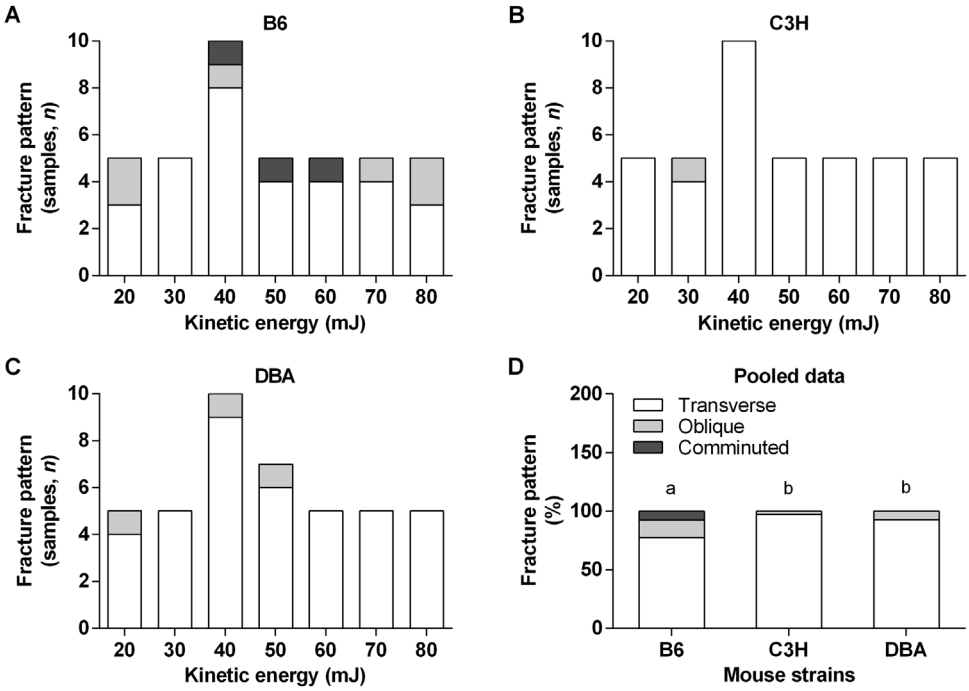

Fig. 6. Fracture patterns for each strain, and pooled results within each strain. A) Fracture patterns in B6 using various kinetic energies; B) Fracture patterns in C3H using various kinetic energies; C) Fracture patterns in DBA using various kinetic energies; D) Fracture patterns using pooled data within the B6, C3H, and DBA strains, $n = 5–10$.

energy, mouse weight, and the structural and material properties of bone characteristic for each strain. We first assessed the phenotypic differences between the strains to determine the correlation between μCT and X-ray derived geometric parameters. Radiographic measurements obtained from plain X-rays were in fact highly correlated with the μCT data, demonstrating the feasibility of using X-ray data to calculate geometric features accurately. This validation was important because the scanning of femurs by μCT without the dissection of soft tissues, while still maintaining the alignment of the fracture fragments, would not have been possible otherwise.

Table 2
Fracture outcomes across the tested mouse strains.

Fracture Outcome	B6	C3H	DBA	Total
Transverse	31 (77.5 %)	39 (97.5 %)	39 (92.9 %)	**109** (**89.3 %**)
Oblique	6 (15.0 %)	1 (2.5 %)	3 (7.1 %)	**10** (**8.2 %**)
Comminuted	3 (7.5 %)	0 (0 %)	0 (0 %)	**3** (**2.5 %**)
Total (*n*)	**40**	**40**	**42**	**122**

The study hypothesis was that the reproducibility of closed transverse fractures would depend on impact kinetic energy and animal body weight, and would be further influenced by phenotypic differences in the femur between these strains. The results demonstrated that closed transverse fractures were reproducibly achieved in all experimental groups under controlled conditions. However, some of the experimental fracture conditions resulted in oblique or comminuted patterns, which more commonly occurred in B6, followed by DBA, and then C3H. It is important to note that no comminuted fractures occurred in the DBA and C3H strains, suggesting that differences in the morphology and material properties of bone in these strains contributed to this outcome. Interestingly, fracture type did not depend on the impact kinetic energy as was hypothesized, but was instead most influenced by the distinct differences in femoral morphology characteristic of each mouse strain. This was in contrast to the study by Marturano et al. [34], where it was reported that the major factor influencing fracture type was impact kinetic energy. These differences are not surprising, and are most likely related to the fact that even the lowest selected parameters used in their

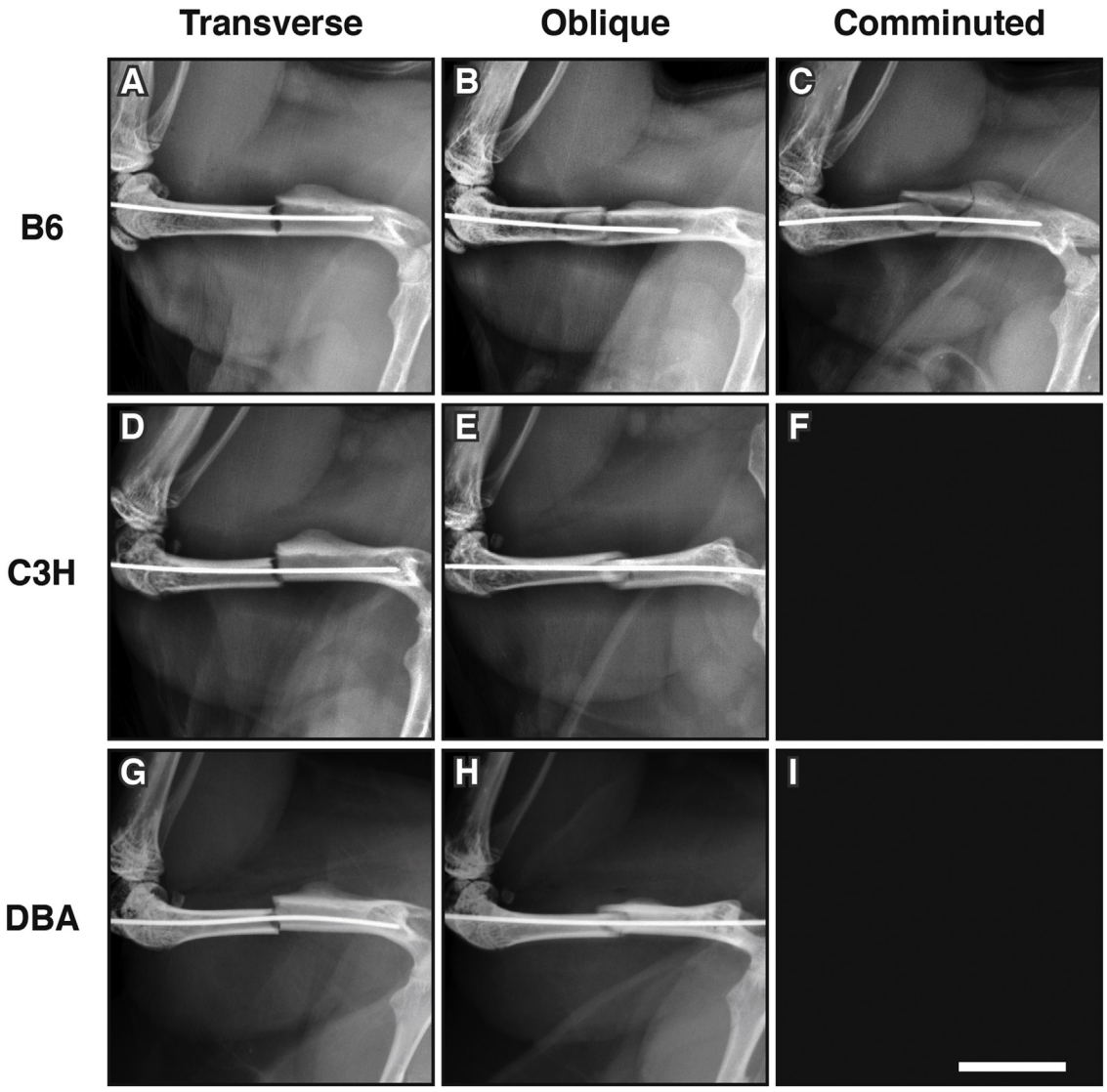

Fig. 7. Representative X-ray images of the fracture patterns for the three tested strains. A) Transverse fracture in B6; B) Oblique fracture in B6; C) Comminuted fracture in B6; D) Transverse fracture in C3H; E) Oblique fracture in C3H; F) No comminuted fractures were observed in C3H with all test conditions; G) Transverse fracture in DBA; H) Oblique fracture in DBA; I) No comminuted fractures were observed in DBA with all test conditions. Scale bar = 5 *mm*.

study, such as drop-weight, velocity, and the resulting kinetic energy, were dramatically greater, 75%, 11%, and 114% respectively, compared to the highest parameters tested in the current study. This is the only other study to our knowledge that attempted to characterize transverse fracture patterns reproducibility in mouse femurs. It is important to emphasize that the results of the current study indicated that having a 200 *g* drop-weight and lower kinetic energies is more than sufficient to reproducibly create closed transverse fractures in mice. Heavy drop-weights and high velocities are unnecessary, and should not be used to avoid oblique and comminuted fracture patterns. Furthermore, it is undoubtedly excessive to use drop-weights of 350–650 *g*, which would result in high kinetic energies on mice that only weigh 22–35 *g*. The current study was in agreement with previous studies demonstrating that the body weight of mice ranging from ~22 to ~34 *g* had no influence on the fracture type outcomes [34].

The most significant finding of this study was that phenotypic differences of the femurs in these mouse strains had the greatest influence on the resulting fracture pattern. The mouse strains selected for this study, B6, C3H, and DBA, each have distinct differences in the structural and material properties of bone [37]. These differences in morphometric properties were corroborated by the resulting fracture patterns observed. For example, BV/TV and CtTh was the lowest in B6, intermediate in DBA, and the highest in C3H, which closely corresponded with the resulting fracture patterns. Accordingly, B6 was the least reproducible, followed by DBA, with C3H having the most reproducible transverse fracture patterns. Bone material properties, such as BMD, is another variable that is often used clinically to determine fracture risk [40], although it is not the only physiological contributor [41–43]. In this study, BMD was significantly lower in B6, and similarly high in DBA and C3H. In contrast to our findings, Beamer et al. reported that BMD was the lowest in B6, followed by DBA, and the highest in C3H, and was significantly different between all of the groups [44]. The reason for the discrepancy of the BMD in the DBA and C3H strains between the studies is not exactly clear, but may be explained by the use of 12 months old mice in Beamer et al. [44] as compared to 3 months old mice in this study. Regardless, it is not surprising that the C3H (97.5%) and DBA (92.9%) strains had more reproducible transverse fractures than B6 (77.5%) as demonstrated by the current study. This was also reflected by the mechanical properties, namely

maximum torque, indicating the contribution of BMD and bone size (TA) to the overall strength of bone. It is possible that better fracture reproducibility in B6 mice could be achieved by further reducing the impact kinetic energy, although this would have to be tested in a follow-up study.

Binomial logistic modelling was also used to assess which variable: kinetic energy, mouse body weight, or BA/TA, would be the best predictor(s) of the resulting fracture pattern. These parameters were chosen due to their previously reported influence on closed fracture outcomes [29,34,37]. This model was able to accurately predict 88.5% of all of the resulting fracture patterns, and confirmed that bone morphometry (BA/TA) was the single strongest predictor of the fracture pattern outcome.

The main limitation of this study was the sample size used to evaluate the reproducibility of fracture patterns ($n = 5, 7$, or 10), as a larger sample size may have resulted in more varied fracture patterns in each strain. Likewise, only a limited range of kinetic energies were assessed, while using parameters outside of the tested range might have resulted in higher numbers of oblique or comminuted fractures. The binomial logistic analysis used to predict fracture outcomes was performed by including mouse femoral structural dimensions measured from radiographic images, with various parameters that were calculated assuming a circular cross-section. Furthermore, the soft tissue of each animal may have also contributed to slight variations in the elevation/depression of the limb, which may have led to magnification differences in radiographic images resulting in minor measurement errors. However, a small number of mouse femurs ($n = 10–12$) were used to determine whether there was a variation in structural parameters assessed by μCT compared to those derived from the X-ray images for each strain. The results confirmed that there was no statistical difference in the calculated values between these imaging modalities, confirming the present model was able to provide an unbiased and accurate analysis that predicted the resulting fracture patterns. It should also be noted that μCT scanning of the mouse femurs prior to creating the fractures is impractical, and hence would not be a suitable assessment method for this type of study.

Conclusion

The results of this study demonstrated that the reproducibility of closed transverse femoral fractures was most strongly influenced by genetic variation rather than the impact kinetic energy or body weight of the mice. This was attributed to differences in the structural and material properties of the bones in each strain. Therefore, special consideration should be taken when planning fracture healing studies using mice with different genetic backgrounds and gene alterations, as the phenotypic differences appear to significantly influence the fracture patterns created. Specifically, using mice that have bones with low BMD, thin cortices, and low BV/TV appeared to be more likely to result in unwanted fracture patterns even at the lowest kinetic energies, as was demonstrated in the B6 mouse strain. Furthermore, this study also demonstrated that the use of lower kinetic energies was more than sufficient to reproducibly create transverse fractures. Although the lowest extremes of kinetic energy were not explored, 20 *mJ* kinetic energy was sufficient to achieve the best reproducibility of fracture patterns across all the strains, regardless of animal body weight. Moreover, the use of a minimal kinetic energy was desirable to minimize soft tissue damage to avoid additional contributions/complications to fracture healing outcomes. Based on these results, unwanted fracture patterns can be avoided by using a lighter drop-weight and lower kinetic energies with a fixed penetration depth (preload) to prevent the rotation of the target limb. The preferred fracture device parameter settings can be determined by using statistical modelling prior to selecting the specific parameters for an *in vivo* study. The creation of reproducible fracture patterns is particularly important as this often dictates the outcomes of fracture healing, and those studies that do not control this potential variability could draw misleading and unwarranted conclusions. These findings are of great benefit for future studies investigating new treatment strategies to improve bone healing, particularly those using murine closed femoral fracture models.

Conflict of interest statement

Co-author Romano Matthys is an employee of RISystem AG Davos, Switzerland that produced the Rodent Fracture Device (RFD).

Acknowledgements

This study was supported by a Start-up grant from the AO Foundation (S-15-155G). We would like to thank Kevin Tetsworth, MD, from The Royal Brisbane Hospital, Australia, for reviewing and commenting on portions of the manuscript.

References

[1] Carlier A, Brems H, Ashbourn JM, Nica I, Legius E, Geris L. Capturing the wide variety of impaired fracture healing phenotypes in Neurofibromatosis Type 1 with eight key factors: a computational study. Sci Rep 2016;7:20010.
[2] Glatt V, Evans CH, Tetsworth K. A concert between biology and biomechanics: the influence of the mechanical environment on bone healing. Front Physiol 2016;7:678.
[3] Havet E, Duparc F, Tobenas-Dujardin AC, Muller JM, Delas B, Freger P. Vascular anatomical basis of clavicular non-union. Surg Radiol Anat 2008;30:23–8.
[4] Santolini E, Goumenos SD, Giannoudi M, Sanguineti F, Stella M, Giannoudis PV. Femoral and tibial blood supply: A trigger for non-union? Injury 2014;45:1665–73.
[5] Simpson AH, Wood MK, Athanasou NA. Histological assessment of the presence or absence of infection in fracture non-union. Injury 2002;33:151–5.
[6] Franco GR, Laraia IO, Maciel AA, Miguel NM, Dos Santos GR, Fabrega-Carvalho CA, et al. Effects of chronic passive smoking on the regeneration of rat femoral defects filled with hydroxyapatite and stimulated by laser therapy. Injury 2013;44:908–13.
[7] Calciolari E, Mardas N, Dereka X, Anagnostopoulos AK, Tsangaris GT, Donos N. The effect of experimental osteoporosis on bone regeneration: part 2, proteomics results. Clin Oral Implants Res 2016.
[8] Calciolari E, Mardas N, Dereka X, Kostomitsopoulos N, Petrie A, Donos N. The effect of experimental osteoporosis on bone regeneration: part 1, histology findings. Clin Oral Implants Res 2016.
[9] de Castro IC, Rosa CB, Dos Reis Junior JA, Moreira LG, Aragao JS, Barbosa AF, et al. Assessment of the use of LED phototherapy on bone defects grafted with hydroxyapatite on rats with iron-deficiency anemia and nonanemic: a Raman spectroscopy analysis. Lasers Med Sci 2014;29:1607–15.
[10] Hamann C, Picke AK, Campbell GM, Balyura M, Rauner M, Bernhardt R, et al. Effects of parathyroid hormone on bone mass, bone strength, and bone regeneration in male rats with type 2 diabetes mellitus. Endocrinology 2014;155:1197–206.
[11] Retzepi M, Lewis MP, Donos N. Effect of diabetes and metabolic control on de novo bone formation following guided bone regeneration. Clin Oral Implants Res 2010;21:71–9.
[12] Rodella LF, Bonazza V, Labanca M, Lonati C, Rezzani R. A review of the effects of dietary silicon intake on bone homeostasis and regeneration. J Nutr Health Aging 2014;18:820–6.
[13] Watkins BA, Li Y, Allen KG, Hoffmann WE, Seifert MF. Dietary ratio of (n-6)/(n-3) polyunsaturated fatty acids alters the fatty acid composition of bone compartments and biomarkers of bone formation in rats. J Nutr 2000;130:2274–84.
[14] Mills LA, Simpson AH. In vivo models of bone repair. J Bone Joint Surg Br 2012;94:865–74.
[15] Takahashi Y, Yamamoto M, Yamada K, Kawakami O, Tabata Y. Skull bone regeneration in nonhuman primates by controlled release of bone morphogenetic protein-2 from a biodegradable hydrogel. Tissue Eng 2007;13:293–300.
[16] Kawaguchi H, Nakamura K, Tabata Y, Ikada Y, Aoyama I, Anzai J, et al. Acceleration of fracture healing in nonhuman primates by fibroblast growth factor-2. J Clin Endocrinol Metab 2001;86:875–80.
[17] Tsuzuki N, Otsuka K, Seo J, Yamada K, Haneda S, Furuoka H, et al. In vivo osteoinductivity of gelatin β-tri-calcium phosphate sponge and bone morphogenetic protein-2 on an equine third metacarpal bone defect. Res Vet Sci 2012;93:1021–5.

[18] McClure SR, Miles K, Vansickle D, South T. The effect of variable waveform low-intensity pulsed ultrasound in a fourth metacarpal osteotomy gap model in horses. Ultrasound Med Biol 2010;36:1298–305.
[19] Cheal EJ, Mansmann KA, DiGioia 3rd AM, Hayes WC, Perren SM. Role of interfragmentary strain in fracture healing: ovine model of a healing osteotomy. J Orthop Res 1991;9:131–42.
[20] Decker S, Reifenrath J, Omar M, Krettek C, Muller CW. Non-osteotomy and osteotomy large animal fracture models in orthopedic trauma research. Orthop Rev (Pavia) 2014;6:5575.
[21] Lu Y, Nemke B, Lorang DM, Trip R, Kobayashi H, Markel MD. Comparison of a new braid fixation system to an interlocking intramedullary nail for tibial osteotomy repair in an ovine model. Vet Surg 2009;38:467–76.
[22] Hart MB, Wu JJ, Chao EY, Kelly PJ. External skeletal fixation of canine tibial osteotomies. Compression compared with no compression. J Bone Joint Surg Am 1985;67:598–605.
[23] Ashhurst DE, Hogg J, Perren SM. A method for making reproducible experimental fractures of the rabbit tibia. Injury 1982;14:236–42.
[24] Waters RV, Gamradt SC, Asnis P, Vickery BH, Avnur Z, Hill E, et al. Systemic corticosteroids inhibit bone healing in a rabbit ulnar osteotomy model. Acta Orthop Scand 2000;71:316–21.
[25] Bonnarens F, Einhorn T. Production of a standard closed fracture in laboratory animal bone. J Orthop Res 1984;2:97–101.
[26] Kokubu T, Hak DJ, Hazelwood SJ, Reddi AH. Development of an atrophic nonunion model and comparison to a closed healing fracture in rat femur. J Orthop Res 2003;21:503–10.
[27] Histing T, Garcia P, Matthys R, Leidinger M, Holstein JH, Kristen A, et al. An internal locking plate to study intramembranous bone healing in a mouse femur fracture model. J Orthop Res 2010;28:397–402.
[28] Cheung KM, Kaluarachi K, Andrew G, Lu W, Chan D, Cheah KS. An externally fixed femoral fracture model for mice. J Orthop Res 2003;21:685–90.
[29] Manigrasso MB, O'Connor JP. Characterization of a closed femur fracture model in mice. J Orthop Trauma 2004;18:687–95.
[30] Holstein J, Menger M, Culemann U, Meier C, Pohlemann T. Development of a locking femur nail for mice. J Biomechanics 2007;40:215–9.
[31] Thompson Z, Miclau T, Hu D, Helms J. A model for intramembranous ossification during fracture healing. J Orthop Res 2002;20:1091–8.
[32] Lybrand K, Bragdon B, Gerstenfeld L. Mouse models of bone healing: fracture, marrow ablation, and distraction osteogenesis. Curr Protoc Mouse Biol 2015;5:35–49.
[33] Histing T, Garcia P, Holstein JH, Klein M, Matthys R, Nuetzi R, et al. Small animal bone healing models: standards, tips, and pitfalls results of a consensus meeting. Bone 2011;49:591–9.
[34] Marturano JE, Cleveland BC, Byrne MA, O'Connell SL, Wixted JJ, Billiar KL. An improved murine femur fracture device for bone healing studies. J Biomech 2008;41:1222–8.
[35] Kratzel C, Bergmann C, Duda G, Greiner S, Schmidmaier G, Wildemann B. Characterization of a rat osteotomy model with impaired healing. BMC Musculoskelet Disord 2008;9:135.
[36] Freeman KT, Koewler NJ, Jimenez-Andrade JM, Buus RJ, Herrera MB, Martin CD, et al. A fracture pain model in the rat: adaptation of a closed femur fracture model to study skeletal pain. Anesthesiology 2008;108:473–83.
[37] Manigrasso MB, O'Connor JP. Comparison of fracture healing among different inbred mouse strains. Calcif Tissue Int 2008;82:465–74.
[38] Jepsen KJ, Price C, Silkman LJ, Nicholls FH, Nasser P, Hu B, et al. Genetic variation in the patterns of skeletal progenitor cell differentiation and progression during endochondral bone formation affects the rate of fracture healing. J Bone Miner Res 2008;23:1204–16.
[39] Jackson R, Reed C, Israel J, Abou-Keer F, Garside H. Production of a standard experimental fracture. Can J Surg 1970;13:415–20.
[40] Hamdy RC. Bone mineral density and fractures. J Clin Densitom 2016;19:125–6.
[41] Karlsson MK, Ahlborg HG, Svejme O, Nilsson JA, Rosengren BE. An increase in forearm cortical bone size after menopause may influence the estimated bone mineral loss–A 28-Year prospective observational study. J Clin Densitom 2016;19:174–9.
[42] Lu J, Shin Y, Yen M-S, Sun SS. Peak bone mass and patterns of change in total bone mineral density and bone mineral contents from childhood into young adulthood. J Clin Densitom 2016;19:180–91.
[43] Gupta Y, Marwaha RK, Kukreja S, Bhadra K, Narang A, Mani K, et al. Relationship between BMD and prevalent vertebral fractures in indian women older than 50 yr. J. Clin. Densitom. 2016;19:141–5.
[44] Beamer WG, Donahue LR, Rosen CJ, Baylink DJ. Genetic variability in adult bone density among inbred strains of mice. Bone 1996;18:397–403.